Open Journal of Applied Sciences, 2026, 16(8), 2682-2705
https://www.scirp.org/journal/ojapps
ISSN Online: 2165-3925
ISSN Print: 2165-3917

Optimizing Recovery Strategies in the Brent East Reservoir of the Alwyn North Field: An Integrated Simulation and Economic Assessment

Franck-Hilaire Essiagne*, Moussa Camara, Kouassi Louis Kra

Laboratoire des Sciences Géographiques du Génie Civil et des Géosciences, Ecole Supérieure de Chimie du Pétrole et de l'Energie (ESCPE), Institut National Polytechnique Félix HOUPHOUET-BOIGNY (INP-HB), Yamoussoukro, Côte d'Ivoire
Email: *franck.essiagne@inphb.ci

How to cite this paper: Essiagne, F.-H., Camara, M. and Kra, K.L. (2026) Optimizing Recovery Strategies in the Brent East Reservoir of the Alwyn North Field: An Integrated Simulation and Economic Assessment. *Open Journal of Applied Sciences*, **16**, 2682-2705.
https://doi.org/10.4236/ojapps.2026.168150

Received: July 16, 2026
Accepted: August 17, 2026
Published: August 20, 2026

Abstract

This study presents an integrated reservoir-simulation and discounted-cash-flow assessment of recovery strategies for the Brent East panel of the Alwyn North Field in the UK Central North Sea. The work uses an ECLIPSE E100 three-dimensional black-oil sector model representing the Brent East panel rather than a complete proprietary full-field model. The corner-point grid contains 36 × 51 × 18 geometrical blocks; the upper zero-porosity interval is inactive, leaving 17 effective reservoir layers representing Tarbert 3, Tarbert 2, Tarbert 1, Ness 2, and Ness 1. Four selected development cases were compared over a 15-year forecast: natural depletion, peripheral water injection, immiscible lean-gas injection, and time-controlled water-alternating-gas injection. The selected natural-depletion case, using five producers and a 5% critical gas saturation, yielded a recovery factor of 26.68%. Water injection with five producers and four injectors increased recovery to 48.61% by maintaining pressure and improving areal sweep. The selected gas case, using three producers and two injectors, achieved 28.16% because early gas breakthrough and an unfavorable gas-oil mobility ratio limited volumetric sweep. WAG, using five producers and six injectors with water and gas assignments switched every two years, delivered the highest technical recovery of 50.73%. Economic results show that water injection has the highest NPV ($1785MM) and IRR (34.78%), whereas gas injection has the shortest payback period (3.703 years). WAG remains technically superior but requires greater investment and operational complexity. No complete observed pressure, oil-rate, water-cut, or GOR time series was available; therefore, the model was not formally history matched, and the results are interpreted as comparative development-screening forecasts. The study demonstrates the value of combining transparent model description, operationally constrained simulation, and economic screening when selecting recovery strategies for heterogeneous Brent-type reservoirs.

Keywords

Brent East, Reservoir Simulation, Natural Depletion, Water Injection, Immiscible Gas Injection, Water-Alternating-Gas, Economic Evaluation, ECLIPSE E100

1. Introduction

Hydrocarbon recovery from mature oil reservoirs remains a major technical and economic challenge because primary and secondary production methods commonly leave a substantial fraction of the original oil in place unrecovered [1] [2]. Reservoir-pressure decline, unfavorable mobility ratios, geological heterogeneity, fault-controlled connectivity, and incomplete areal and vertical sweep can shorten production plateaus and reduce project value [3]-[5]. As the discovery of large conventional reservoirs becomes less frequent, optimizing recovery from existing fields is increasingly important for extending field life, sustaining infrastructure use, and maximizing asset value [1] [6]. Enhanced oil recovery and pressure maintenance processes therefore play a central role in development planning [4] [7] [8].

Reservoir simulation is widely used to evaluate multiphase-flow behavior, forecast production, test well configurations, and compare field-development strategies under complex geological and operational conditions [9]-[13]. A numerical model integrates structural geometry, porosity, permeability, saturation functions, fluid properties, well controls, and facility constraints. Compared with simplified analytical calculations, simulation can represent spatial variations in pressure support, phase mobility, breakthrough, and well interference [4] [6] [12] [13]. Nevertheless, simulation forecasts are only as reliable as their input data, calibration, and reporting. Reproducible studies must therefore disclose grid architecture, initialization volumes, fault treatment, well controls, and uncertainty limitations.

Water injection, gas injection, and water-alternating-gas injection are among the most frequently evaluated methods for maintaining pressure and mobilizing additional oil. Water injection usually improves macroscopic sweep and suppresses free-gas evolution when reservoir pressure is maintained above bubble point [10] [12] [14]. Gas injection may improve microscopic displacement through oil swelling, viscosity reduction, and solution-gas effects, but low gas viscosity can cause gravity override, channeling, and early gas breakthrough [3] [7] [15]. WAG combines the displacement contribution of gas with the mobility-control and pressure-support benefits of water; its performance depends on heterogeneity, relative permeability, phase trapping, well pattern, and cycle design [5] [8] [16].

The Alwyn North Field lies in the UK Central North Sea and contains structurally segmented Brent Group reservoirs with variable depositional facies and reservoir quality [17]-[22]. Hydrocarbons occur mainly in Middle Jurassic sandstones of the Tarbert and Ness formations, which have contrasting connectivity, saturation, and displacement characteristics [20] [21] [23]-[29]. The broader Alwyn North Field includes several fault-bounded panels with different pressure regimes and fluid contacts; consequently, conclusions from one sector should not automatically be extrapolated to the entire field.

Previous studies have compared natural, water-drive, and gas-drive behavior in Alwyn North or analogous Brent-type reservoirs [9] [17]. Other work has investigated waterflood optimization, injectivity decline, WAG mechanisms, EOR screening, data-driven EOR selection, and the effects of heterogeneity on multiphase displacement [8] [10] [12]-[14] [16] [30]-[33]. However, fewer studies present natural depletion, water injection, immiscible gas injection, and WAG within a single technical-economic framework while also reporting the operational constraints and model limitations that control the comparison.

The present study is restricted to the Brent East panel of the Alwyn North Field. It uses a Brent East sector model and selected development cases reconstructed from the available model records, simulation outputs, and economic calculations. The objectives are to: i) describe the model and data provenance sufficiently for technical assessment; ii) compare selected natural-depletion, water-injection, gas-injection, and WAG cases under common constraints; iii) integrate recovery, well count, operability, and discounted economics; and iv) identify the most technically effective and economically attractive strategy without presenting the sector model as a history-matched full-field prediction.

2. Geological Setting

The Alwyn North Field is located in the southeastern East Shetland Basin, approximately 140 km east of the Shetland Islands, within UKCS Blocks 3/9 and 3/4 and in about 130 m of water [17] [19] [20]. The field occupies an intermediate structural terrace between the East Shetland Platform and the Viking Graben. Regional extensional tectonism generated a complex fault pattern, while erosion at the Base Cretaceous Unconformity modified the eastern part of the Brent succession [17] [19].

Seismic interpretation divides the broader field into several structural and stratigraphic panels, including Brent North, Brent Northwest, Brent Southwest, Brent East, Statfjord, and Triassic compartments. RFT observations and different water-oil contacts indicate that the wider panels may have distinct pressure regimes. The present simulation does not represent all of these compartments; it focuses only on Brent East.

The Brent East structure is an eroded monoclinal bounded by the Base Cretaceous Unconformity to the east and south, the Spinal Fault to the west, and a northern fault of locally small throw. The hydrocarbon accumulation is therefore controlled by both structural and stratigraphic trapping. Within the sector model, one SW-NW fault is documented as communicating and one N-S fault as sealing. The available model records are not fully consistent on equilibration contacts: one description indicates a common initial pressure and water-oil contact for the three regions, whereas another initialization record displays WOCs of 3231, 2900, and 3247 m for regions 1 - 3. Because the final ECLIPSE deck was unavailable, the contact definition actually used in the selected simulations cannot be independently verified.

The Middle Jurassic Brent Group records deltaic to shallow-marine deposition and comprises Lower Brent, Ness, and Tarbert units. Tarbert 3 contains laterally extensive, high-quality shoreface sands; Tarbert 2 contains more micaceous lower-permeability sandstones; Tarbert 1 contains comparatively clean reservoir sandstone. Ness 2 contains heterogeneous delta-plain and lagoonal sand bodies interbedded with shale and coal, whereas Ness 1 contains poorer reservoir intervals and relatively little oil in the eastern part of the sector [21] [23]-[26]. These depositional contrasts create vertical and lateral variability in porosity, permeability, capillary pressure, and relative permeability.

Reservoir quality in published Brent Group studies commonly falls in the 15% - 25% porosity and 100 - 500 mD permeability ranges, although local values vary with facies and diagenesis [18] [21] [24]-[26] [28]. Tarbert generally provides better lateral communication and higher initial oil saturation, whereas Ness contains discontinuous sand bodies and more water-bearing volume. The Heather Formation, Kimmeridge Clay, and overlying Cretaceous succession provide regional sealing [17] [20] [21].

The distinction between the complete Alwyn North Field and the modeled Brent East panel is maintained throughout this study. Field-level geological publications are used to describe regional context, whereas model-specific geometry, layer architecture, well configurations, and schedules are derived from the available sector-model records. The regional location is shown in **Figure 1**, and the structural and stratigraphic context of the Brent East panel is shown in **Figure 2**.

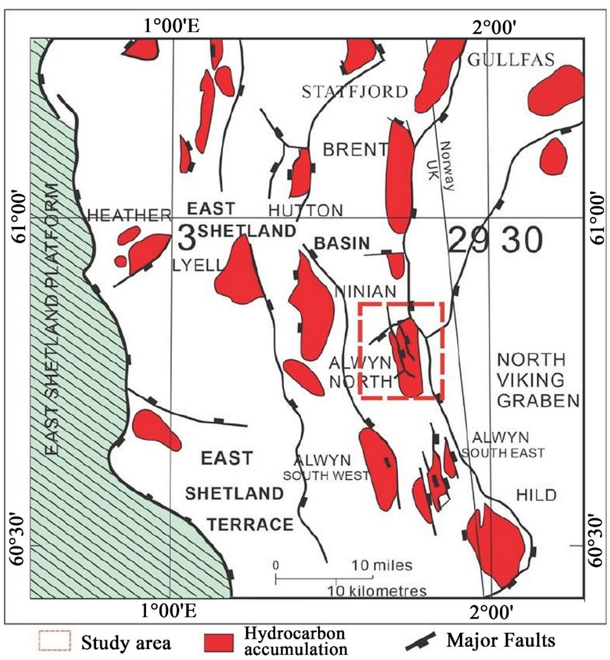

Figure 1. Location of the Alwyn north field in the east Shetland basin.

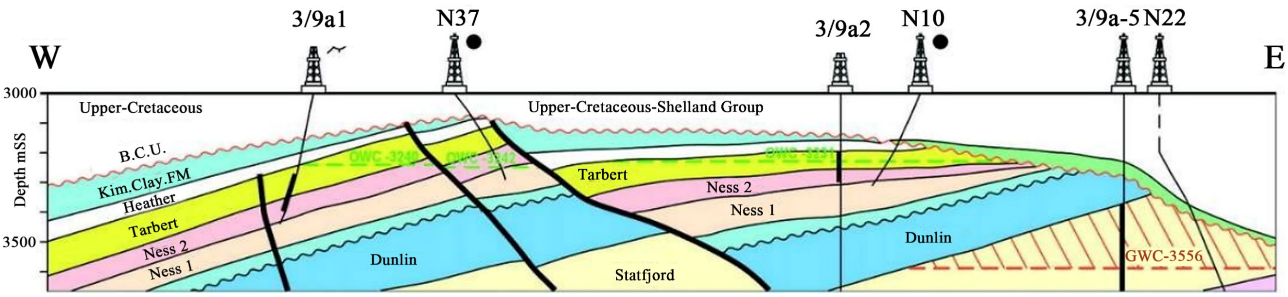

Figure 2. Structural and stratigraphic context of the Brent East panel and the Tarbert-Ness reservoir interval.

3. Methodology

The study combined analytical screening, numerical reservoir simulation, and discounted cash flow analysis. Analytical calculations were used to estimate recovery and preliminary well requirements. ECLIPSE E100 simulations were then used to test well configurations and operational controls. The selected cases were compared using recovery factor, pressure behavior, oil-rate plateau, water cut, GOR, well count, investment, NPV, IRR, and payback period. The same 15-year economic basis was applied to all selected cases.

3.1. Reservoir Model, Grid, and Data Provenance

The dynamic model is an ECLIPSE E100 black-oil sector model for the Brent East panel. It is not a proprietary full-field Alwyn North model and was not constructed independently from raw seismic and well data for this paper.

The supplied model inputs comprise corner-point geometry, upscaled petrophysical properties, PVT tables, relative permeability and capillary pressure functions, equilibration regions, and appraisal-well definitions. This study modified well configurations, critical gas saturation, production and injection controls, and economic cases during scenario screening. Table 1 summarizes the model architecture, initialization parameters, and data provenance. The archived materials do not include the original ECLIPSE DATA/GRID deck or a simulator printout listing ACTNUM totals and explicit fault multipliers. The exact active-cell count and numerical transmissibility multipliers therefore cannot be reported. The source documents also use different layer-indexing and WOC descriptions; Table 1 discloses these differences rather than assigning unsupported deck-level values. The three-dimensional grid and appraisal-well representation are illustrated in Figure 3.

Table 1. Model architecture and data provenance.

Parameter	Value/status	Provenance and interpretation
Model scope	Brent East panel of Alwyn North	Supplied Brent East sector model; not the complete field
Simulator/fluid representation	ECLIPSE E100, three-phase black oil	Supplied sector model
Geometrical grid	36 × 51 × 18 = 33,048 blocks	Corner-point geometry in MODEL_PETREL.GRDECL

Continued

Effective reservoir-layer interpretation	Available model description: 36 × 51 × 17 = 31,212 reservoir-layer blocks before additional ACTNUM masking	Upper BCU-Top Brent interval is zero porosity; an alternative archived rock-type convention retains 18 layer indices
Nominal cell dimensions	110 m × 205 m × 15 m	Available model documentation
Exact ACTNUM-active count	Not recoverable from available archived records	No unsupported active-cell number is assigned
Tarbert/Ness layer architecture	Available layer description: T3/T2/T1 = 3/2/3; N2/N1 = 5/4 layers	Alternative archived indexing: Tarbert 1 - 9, Ness 10 - 16, Lower Brent 17 - 18; final deck unavailable to reconcile indexing
Fault representation	SW-NW communicating fault; N-S sealing fault	Binary behavior documented; explicit numerical multipliers unavailable
Equilibration regions/WOC	Three regions; source descriptions conflict	One archived description indicates common pressure/WOC; another displays WOCs of 3231, 2900, and 3247 m; final deck unavailable
Appraisal wells represented	A2, A4, N2, N3	Supplied well definitions
Water-oil contact	Not independently verified for selected deck	See equilibration-region disclosure above
OOIP	35.665 million Sm^3	ECLIPSE field-total initialization
Average field porosity/permeability	0.160/233.8 mD	Available property summary
Scenario choices	Well counts, new-well roles, A2 conversion, Sgc = 5%, injection schedules	Selected in this study after scenario screening

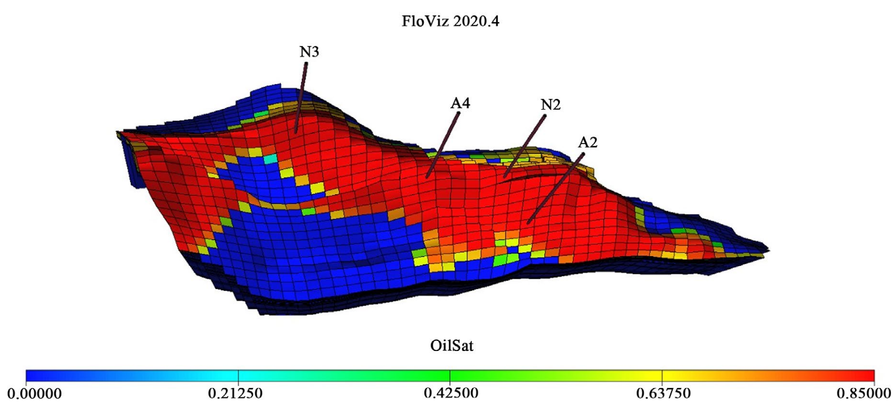

Figure 3. Three-dimensional Brent East simulation grid and appraisal-well representation.

3.2. Petrophysical, Fluid, and Saturation Functions

Porosity, permeability, net-to-gross, and facies properties were upscaled into the simulation grid. Deterministic trend-controlled modeling was used for laterally extensive Tarbert and shallow-marine sandstones, whereas object-based concepts were used for heterogeneous Ness floodplain and lagoonal elements. The available property summary gives a field-average porosity of 0.160 and average permeability of approximately 234 mD, with higher average porosity in the principal oil-bearing region than in the more water-prone region.

The black-oil fluid model uses pressure-dependent oil formation-volume factor, solution gas-oil ratio, oil viscosity, gas formation-volume factor, gas viscosity, and water properties. Initial pressure is approximately 446 bar and the saturated-oil table reaches a solution GOR of 206.897 Sm^3/Sm^3 at 258.236 bar. The value 206.897 is therefore a solution GOR, not a bubble-point pressure. The bubble-point pressure used in the numerical model is approximately 258.24 bar. Water formation-volume factor is 1.047 rm^3/Sm^3, water viscosity is 0.27 cp, and water compressibility is 5.0×10^{-5} bar^{-1}.

Separate oil-water and gas-oil saturation functions are assigned to Tarbert and Ness rock types. Tarbert has lower connate-water saturation and more favorable oil-water displacement than Ness. Critical gas saturation (Sgc) was examined during natural-depletion screening. A value of 5% was retained as the selected sensitivity case because it delayed free-gas mobility and improved production continuity relative to the zero-Sgc cases. Because historical GOR and pressure data were unavailable, Sgc = 5% is an uncalibrated sensitivity assumption rather than a history-matched field parameter.

3.3. Numerical Water Support and Model Verification

No separate Carter-Tracy or Fetkovich analytical aquifer was documented in the archived model description. Pressure support is represented by explicitly gridded water-bearing cells located below and adjacent to the oil-bearing interval and connected through the reservoir grid. Their contribution depends on pore volume, porosity, compressibility, permeability, saturation, and transmissibility. The available numerical water-support parameters are summarised in Table 2.

Table 2. Numerical water-support description and available parameters.

Water-support item	Value/status	Interpretation
Aquifer representation	Explicit gridded water-bearing cells	No separate analytical aquifer documented
Field pore volume at reference conditions	385,365,518 rm^3	ECLIPSE field-total PORV from initialization summary
Original water in place	313,764,608 Sm^3	ECLIPSE field-total originally-in-place water value
Initial water-oil contact	Source conflict; final deck unavailable	Archived model descriptions contain conflicting WOC definitions
Water salinity	Approximately 17,000 ppm	Available model documentation
Water-zone-specific pore volume	Not separately recoverable	Field total is reported; aquifer-only value unavailable
Cumulative water influx diagnostic	Not archived as a separate aquifer summary	Water production and pressure response are discussed qualitatively
Calibration against observed influx	Not performed	No complete observed pressure/water history available

A formal history match was not performed. The archived development-planning dataset does not contain complete observed time series for reservoir or well pressure, oil rate, water cut, and GOR. Consequently, quantitative history-match errors and acceptance criteria cannot be reported. Model checks were limited to initialization-volume review, consistency of PVT and saturation tables, material-balance comparisons, well-control verification, facility-limit checks, and qualitative assessment of pressure, water-cut, and GOR trends. The availability of each requested historical variable and the verification scope are summarised in Table 3.

Table 3. History-data availability and verification scope.

Requested variable	Historical data available?	Treatment in this study
Pressure	No complete observed series	Initialization and forecast-trend checks only
Oil rate	No complete observed series	Scenario production and facility-limit checks
Water cut	No complete observed series	Forecast trend and 90% limit
GOR	No complete observed series	Forecast trend and 1500 Sm^3/Sm^3 limit
Cumulative oil	No historical calibration series	Cross-check of simulator recovery factors and economic cases
History-match acceptance criteria	Not applicable	No formal history matching was undertaken

The results are therefore interpreted as internally consistent comparisons among development strategies under a common sector model, not as deterministic full-field forecasts. This limitation is important because inverse modeling and data assimilation can materially change fault transmissibility, aquifer strength, and permeability distributions when production history becomes available [34] [35].

3.4. Development Scenarios and Operational Controls

Four selected numerical cases were retained after screening alternative well counts and operating choices. Natural depletion uses a 100-bar minimum producer BHP and a 3200 Sm^3/d field plateau. Secondary-recovery producers use a 260-bar minimum BHP. The maximum water-injection rate is 3000 Sm^3/d per well and 15,000 Sm^3/d for the field. The maximum gas-injection rate is 800,000 Sm^3/d per well and 3,200,000 Sm^3/d for the field. Injection is controlled by voidage replacement, and injector pressure must remain below the approximate 480-bar fracture-pressure limit.

Table 4 lists the selected configurations and controls, Table 5 records the preserved well roles and placement information, Figure 4 shows the peripheral water-injection layout, and Figure 5 shows the alternating-phase injector schedule.

The WAG case uses a time-controlled alternating-phase well schedule rather than a conventional fixed-slug design. Individual injector roles are switched between water and gas at approximately two-year intervals. Actual water and gas rates vary under voidage-replacement, pressure, and injectivity constraints; therefore, a single fixed hydrocarbon-pore-volume slug size or WAG ratio cannot be reconstructed from the preserved documentation.

Table 4. Selected development cases and operating controls.

Scenario	Selected configuration	Start logic	Rate/plateau control	Additional constraints
Natural depletion	5 producers; A2 shut	Production from model start	3200 Sm^3/d plateau; minimum BHP 100 bar	Sgc = 5% selected sensitivity; not history calibrated; field economic limit 1000 Sm^3/d
Water injection	5 producers + 4 injectors; A2 converted plus 3 new peripheral injectors	28 Oct. 2025, after about 2.5 years depletion at ~293 bar	5,000 Sm^3/d oil plateau; water ≤ 3000 Sm^3/d/well and ≤ 15,000 Sm^3/d field	Voidage replacement; producer BHP ≥ 260 bar; fracture-pressure limit ~480 bar
Immiscible gas injection	3 producers + 2 new gas injectors	After initial depletion; exact selected-case calendar date not recoverable	Gas ≤ 800,000 Sm^3/d/well and ≤ 3,200,000 Sm^3/d field	Voidage replacement; lean Statfjord gas represented as Brent dissolved gas; miscibility not demonstrated
WAG injection	5 producers + 6 injectors	Six injectors commissioned after depletion during 2025-2026 in the available schedule record	I1-I3 initially water; I4-I6 initially gas; assignments switch every 2 years	Time-controlled alternating-phase well schedule; no fixed pore-volume slug or prescribed WAG ratio

Table 5. Preserved well identities and placement information.

Scenario	Well roles and location description	Completion/placement information
Natural depletion	A4, N2, N3 plus P1 and P2 produce; A2 is shut	Oil-bearing Tarbert-Ness interval; exact I/J/K and completion cells unavailable
Water injection	A4, N2, N3, P1, P2 produce; A2 plus three new injectors form a peripheral pattern	Injection mainly targets Tarbert; exact new-well grid coordinates unavailable in the available records
Gas injection	A4, N2, N3 produce; two new gas injectors	Gas restricted to oil-bearing Tarbert; exact grid coordinates unavailable
WAG injection	Five producers; injectors I1-I3 and I4-I6 alternate water/gas roles	Initial phase allocation and two-year switching preserved; exact I/J/K completion cells unavailable

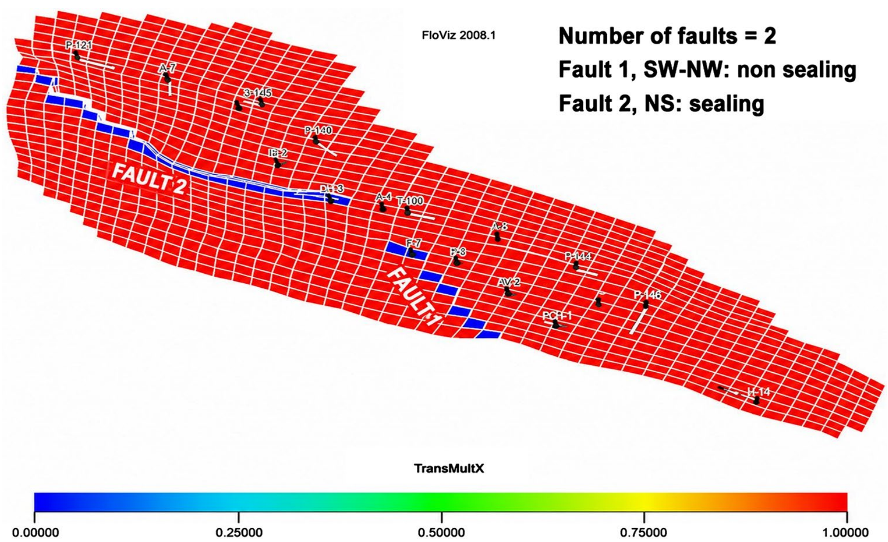

Figure 4. Peripheral water-injection layout used during scenario screening; the selected case converts A2 and uses three additional peripheral injectors.

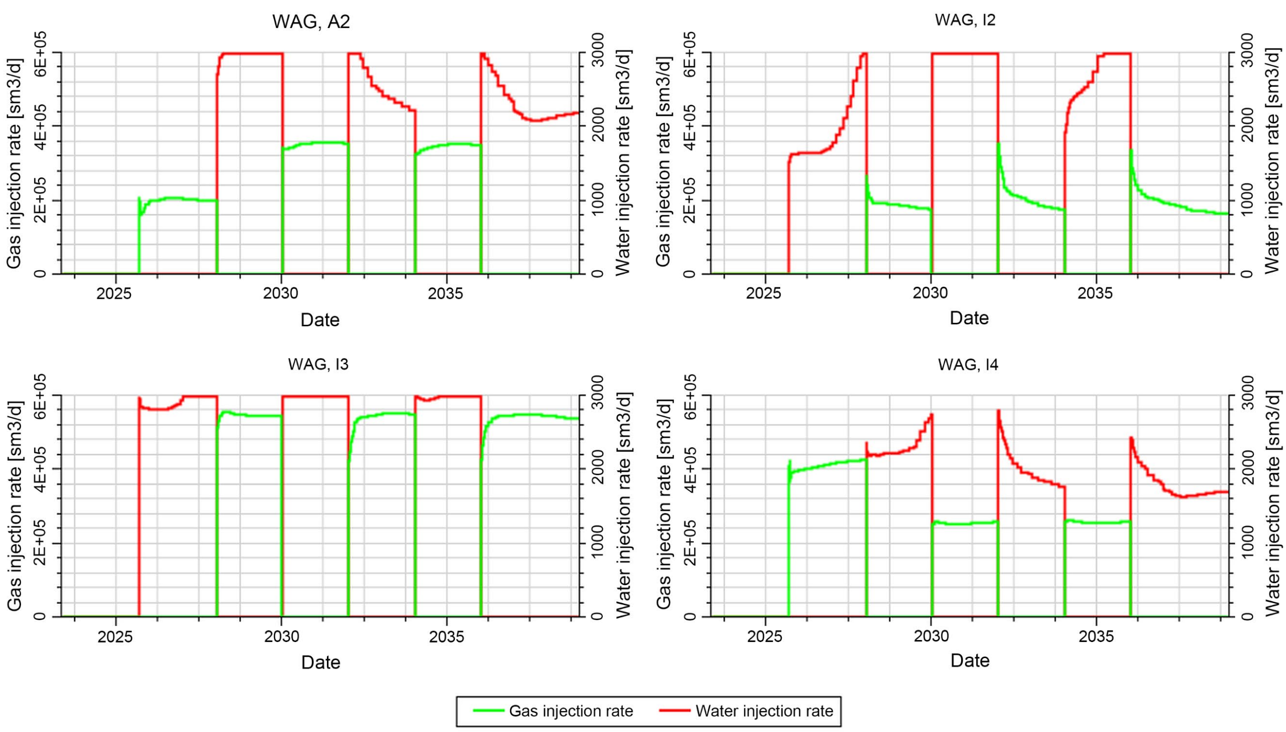

Figure 5. Time-controlled alternating-phase injector schedule: I1-I3 initially inject water and I4-I6 gas, with individual well roles switched at approximately two-year intervals.

3.5. Economic Evaluation

Economic performance was calculated from the selected simulation production profiles over a 15-year project life. Revenue used a March 2023 Brent oil price of 85.38 USD/bbl. Lifting, production, and transportation cost was 10 USD/bbl. The discount rate was 10% and income tax was 40%. Linear depreciation was applied in the economic calculations. Capital costs included common platforms and facilities, scenario-specific wells, and gas compression where required. The economic assumptions are listed in Table 6.

Table 6. Economic assumptions used in the analysis.

Economic item	Assumption
Oil price	85.38 USD/bbl
Project life	15 years
Discount rate	10%
Income tax	40%
OPEX	10 USD/bbl
Treatment and production facilities platform	700 MM$
Drilling and accommodation platform	250 MM$
Secondary platform	250 MM$ when required
Deviated platform well	12 MM$/well
Horizontal platform well	16 MM$/well
Vertical subsea well and piping	36 MM$/well
Horizontal subsea well and piping	40 MM$/well
Installed gas compressor	44.2 MM$

The reported economic calculation labels NPV divided by total investment as the profitability index. Because this differs from the conventional present-value-of-inflows definition, the metric is reported here as the NPV/investment ratio and is defined explicitly as NPV divided by total investment. Table 7 reconciles the reported scenario investments, and Table 8 lists the economic calculation definitions. Economic ranking considers NPV, IRR, payback, recovery, and implementation requirements rather than payback period alone. The reported capital totals are reconciled in Table 7, and the editable economic equations are provided in Table 8.

Table 7. Scenario-level capital-investment reconciliation.

Cost component (MM$)	Natural depletion	Water injection	Gas injection	WAG injection
Common treatment/production and drilling/accommodation facilities	950	950	950	950
Scenario-specific drilling, completion, compression, and other recorded capital	120	228	128	344
of which installed gas compressor is identified	0	0	44.2	44.2
Reported total investment	1070	1178	1078	1294

Note: The available cost summary gives a common 950 MM$ facilities cost and the total scenario investments. The gas and WAG scenario-specific amounts include the 44.2 MM$ installed compressor. A more detailed allocation of the WAG balance was not preserved.

Table 8. Economic calculation definitions used in this study.

Quantity	Definition
Annual revenue	$R_t = Q_{o,t} \times P_o$
Annual OPEX	$OPEX_t = Q_{o,t} \times C_o$
Straight-line depreciation	$D = \dfrac{I_{dep}}{n}$
Taxable income	$TI_t = R_t - OPEX_t - D_t$
Tax	$T_t = 0.40 \times TI_t$
Net cash flow	$CF_t = R_t - OPEX_t - T_t - CAPEX_t$
NPV	$NPV = \sum_{t=0}^{n} \dfrac{CF_t}{(1+i)^t}$
IRR	$0 = \sum_{t=0}^{n} \dfrac{CF_t}{(1+IRR)^t}$
Payback period	$PBP = t + \dfrac{-CCF_t}{CF_{t+1}}$
Reported NPV/investment ratio	$PI_{reported} = \dfrac{NPV}{I_{total}}$

4. Results and Discussion

The selected cases show that recovery in the Brent East sector is controlled by the interaction of pressure support, phase mobility, reservoir heterogeneity, well configuration, and facility constraints. Natural depletion is limited by pressure decline and free-gas mobility. Water injection provides the largest economically efficient increment through pressure maintenance and areal sweep. Continuous gas injection is constrained by early gas breakthrough. WAG provides the highest recovery but only a modest increment above waterflooding and requires more wells, compression, and operating intervention.

4.1. Natural-Depletion Performance

Natural depletion was first evaluated as the reference case. The principal energy contributions are fluid and rock expansion, solution-gas behavior below bubble point, and influx from connected water-bearing grid cells. An analytical material-balance calculation that neglected water influx and spatial heterogeneity gave a recovery factor of approximately 5.68%. This analytical value is not used as the selected numerical forecast; it provides a lower-complexity screening estimate [34] [36].

The selected numerical case uses five producers and Sgc = 5% and maintains the 3200 Sm^3/d plateau for approximately six years before declining as pressure and deliverability decrease. The selected recovery factor is 26.68%. The higher numerical result relative to the simplified analytical calculation reflects three-dimensional property variation, well placement, relative-permeability behavior, and pressure support from the gridded water zone. It should not be interpreted as a history-matched measure of aquifer strength or Sgc.

Well performance is heterogeneous. A2 was shut because of poor oil contribution and adverse water behavior, whereas additional producers improved areal access to oil-bearing cells. Below bubble point, liberated gas reduces oil relative permeability and increases GOR. The 5% critical gas saturation delays gas mobility and improves production continuity compared with the zero-critical-gas-saturation cases. Pressure nevertheless approaches the 100-bar BHP constraint late in the forecast, and more than 70% of OOIP remains in place.

Comparison with previous studies. The inferior performance of primary depletion relative to injection agrees qualitatively with the Alwyn North drive-mechanism comparison reported by Amadi *et al.* [9] and with broader EOR reviews showing that expansion and solution-gas drive generally leave large mobile-oil volumes in heterogeneous reservoirs [1] [8]. The difference between the 5.68% analytical estimate and the 26.68% numerical case also illustrates the limits of simplified material balance when water influx and spatially variable flow are not explicitly represented [34] [36] [37]. The natural-depletion responses are shown in **Figure 6**.

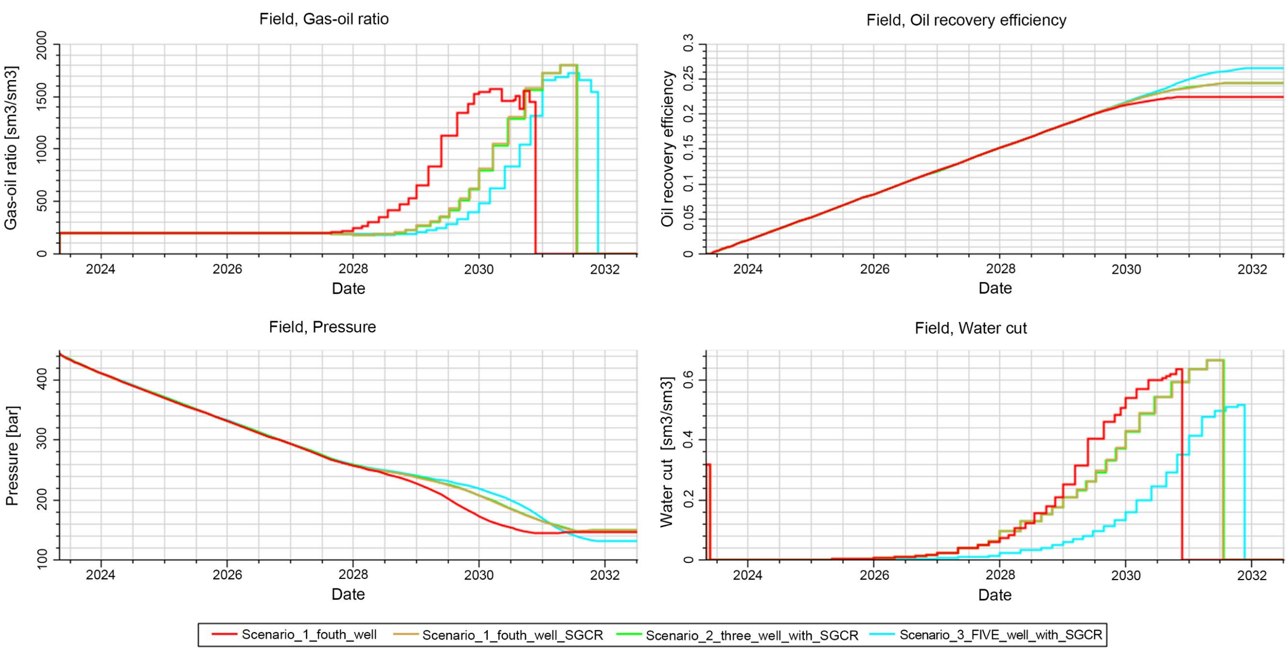

Figure 6. Natural-depletion scenario screening showing GOR, oil rate, recovery factor, pressure, and water-cut responses.

4.2. Water-Injection Performance

Peripheral water injection is initiated on 28 October 2025, approximately 2.5 years after production begins, when average reservoir pressure has declined to about

293 bar. This start point is above the 258.24-bar bubble point and is intended to limit free-gas evolution while allowing a short natural-depletion period. A2 is converted from a shut producer to an injector and three additional peripheral injectors are added, giving five producers and four injectors in the selected case.

The selected waterflood reaches a recovery factor of 48.61%, a 21.93-percentage-point increment above natural depletion. The 5000 Sm^3/d oil plateau is maintained for about seven years and field life extends to approximately fourteen years. Reservoir pressure remains above the secondary-recovery BHP limit, and GOR stays comparatively stable because pressure is maintained near or above bubble point for much of the forecast. The water-injection rate is initially high to replace the voidage created before injection and declines with production demand.

The Tarbert interval responds more favorably than the Ness interval because Tarbert has higher initial oil saturation, cleaner connected sandstone, and more favorable oil-water fractional-flow behavior. Ness contains more heterogeneous, water-prone facies and therefore retains more bypassed oil after breakthrough. This contrast demonstrates that permeability alone does not determine recovery; initial saturation, connectivity, relative permeability, and contact with injectors are also important.

Water cut increases after breakthrough and is highest in the existing producers A4, N2, and N3. The field is ultimately constrained by the 90% water-cut limit and the 1000 Sm^3/d field economic rate. Scenario screening showed that the four-injector case using A2 achieved comparable or slightly better recovery than the five-injector alternatives while requiring one fewer new well. The resulting reduction in drilling expenditure is a principal reason for its economic advantage.

Comparison with previous studies. The improvement from 26.68% to 48.61% is consistent with published waterflood studies showing that pressure maintenance and improved areal sweep can approximately double recovery relative to unsupported depletion in suitably connected sandstone reservoirs [10] [12]. The observed rise in water cut and the need to balance voidage replacement against premature breakthrough also agree with field and optimization studies of water-injection performance [12] [14]. In the Brent context, laterally connected Tarbert shoreface sands are expected to respond more uniformly than heterogeneous Ness delta-plain deposits [21] [23]. The selected water-injection responses are shown in **Figure 7**.

4.3. Immiscible-Gas-Injection Performance

The economically selected gas case uses three producers and two new injectors. Lean Statfjord gas is assigned properties comparable with Brent dissolved gas, but no minimum-miscibility-pressure study demonstrates miscibility. The process is therefore described as immiscible gas injection. Gas is injected under voidage-replacement control with a per-well limit of 800,000 Sm^3/d and field limit of 3.2 million Sm^3/d.

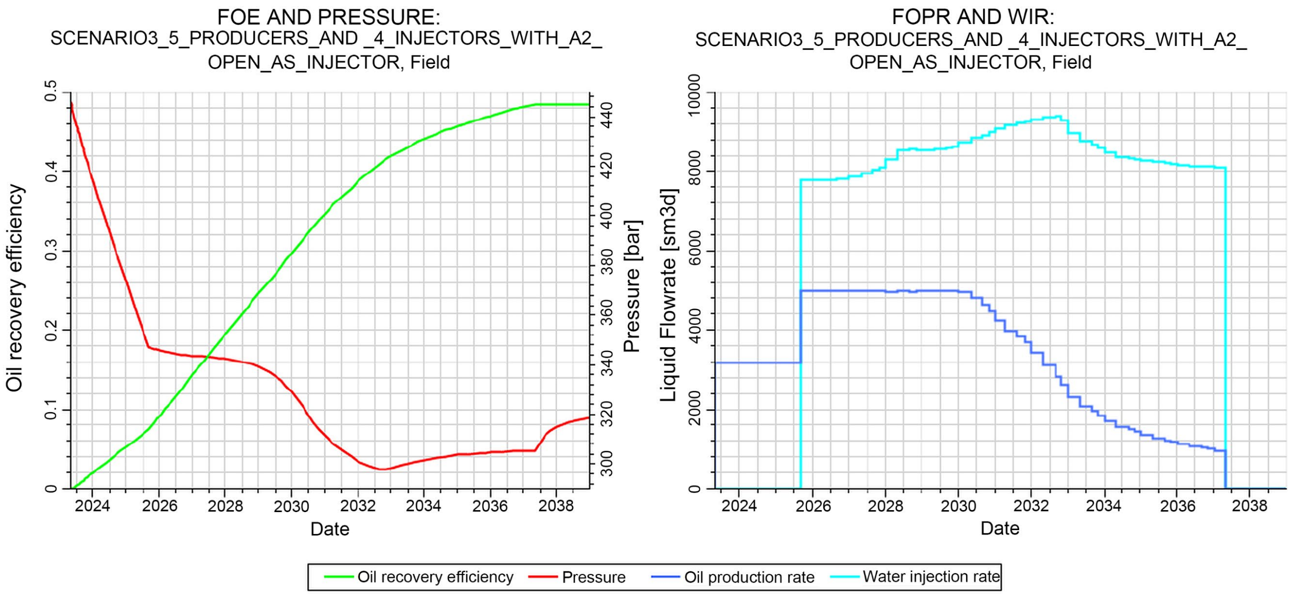

Figure 7. Selected water-injection case with five producers and four injectors, including A2 converted to injection.

The selected recovery factor is 28.16%, only 1.48 percentage points above natural depletion and substantially below water injection. Gas initially supports pressure and can dissolve in oil, but the low gas viscosity produces an unfavorable mobility ratio. Preferential gas flow through connected high-permeability cells causes early breakthrough, rapid GOR escalation, gas override, and incomplete volumetric sweep. The Ness interval is not a favorable gas target because much of it is water bearing and heterogeneous.

The selected archived case reaches a peak GOR of approximately 1570 Sm^3/Sm^3, slightly above the stated 1500 Sm^3/Sm^3 facility/economic limit. The preserved case did not implement a hard shut-in at the first exceedance; the exceedance is therefore treated as an operational limitation rather than evidence of strict compliance with the limit. Field implementation would require gas-handling debottlenecking, tighter well controls, or earlier curtailment.

The gas case uses fewer wells and consequently has a relatively low investment and the shortest payback period. However, its NPV and recovery remain much lower than those of the water and WAG cases. The case demonstrates that a short payback does not necessarily identify the highest-value recovery strategy when incremental reserves are limited.

Comparison with previous studies. The modest recovery increment and rapid GOR increase are consistent with immiscible gas-injection behavior in heterogeneous reservoirs, where low gas viscosity and density encourage channeling and gravity segregation [3] [7] [8] [15]. The findings also agree with the Alwyn North drive comparison of Amadi *et al.* [9], in which gas-drive performance was constrained by mobility and breakthrough. These mechanisms motivate the use of alternating water to improve mobility control [16]. The selected immiscible-gas responses are shown in **Figure 8**.

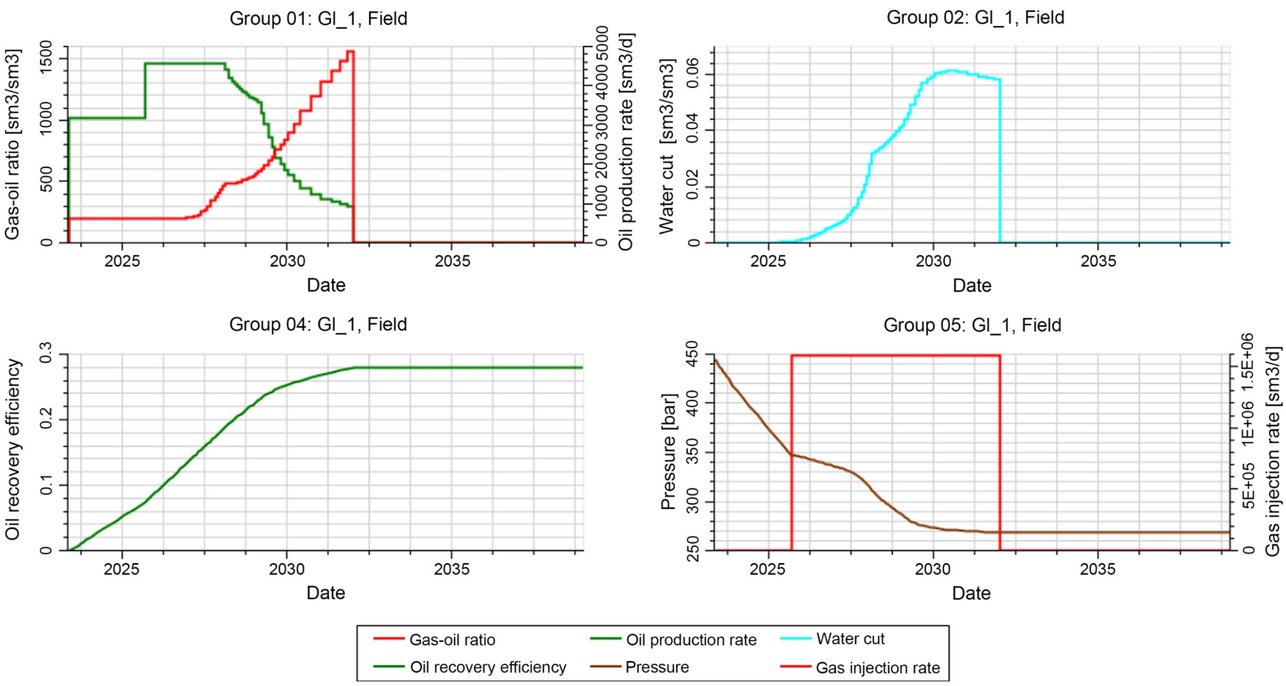

Figure 8. Selected immiscible-gas case with three producers and two injectors.

4.4. Water-Alternating-Gas Performance

The WAG case uses five producers and six injectors. I1-I3 initially inject water and I4-I6 initially inject gas; individual injector roles switch at approximately two-year intervals and continue to alternate. This is a time-controlled alternating-phase well schedule rather than a fixed pore-volume-slug design. Water and gas rates vary under voidage-replacement, pressure, and injectivity constraints.

WAG produces the highest selected recovery factor, 50.73%. Water phases reduce gas mobility and improve areal sweep, while gas phases contribute oil swelling and viscosity reduction. The alternating pattern limits some of the channeling observed in continuous gas injection and contacts bypassed oil more effectively. Pressure remains substantially more stable than under natural depletion and gas-only injection.

The incremental recovery above water injection is 2.12 percentage points. This gain is technically meaningful but much smaller than the 21.93-percentage-point waterflood increment above natural depletion. WAG also requires six injectors, gas compression, phase switching, and more complex surveillance. The archived case shows variable water injectivity, which may reflect changing relative permeability, phase trapping, scale risk, or near-well impairment. These effects would require additional laboratory and field investigation before implementation.

Comparison with previous studies. The improvement of WAG over continuous gas injection is consistent with the main mechanism reported in the WAG literature: water reduces effective gas mobility and redistributes flow, while gas improves microscopic displacement [8] [16]. The relatively small increment over waterflooding is also plausible in a reservoir where water injection already produces strong pressure maintenance and areal sweep. Published reviews emphasize that WAG performance is reservoir-specific and may be limited by phase trapping, heterogeneity, injectivity loss, and operating complexity [16]. The selected WAG responses are shown in Figure 9.

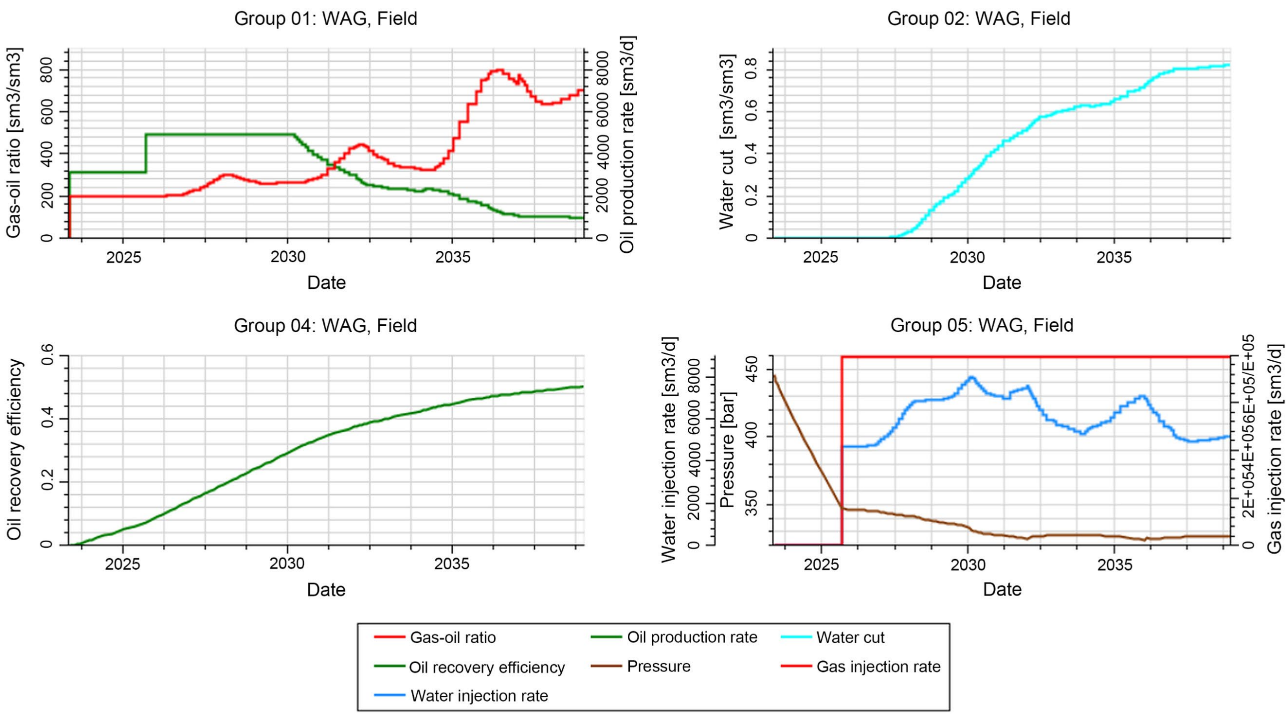

Figure 9. Selected WAG case showing oil rate, GOR, water cut, recovery factor, pressure, and alternating injection responses.

4.5. Integrated Technical-Economic Assessment

The selected-case well counts and recovery factors are summarised in Table 9 and Figure 10, respectively.

Table 9. Technical comparison of the selected numerical cases.

Scheme	Producers	Injectors	Recovery factor (%)	Increment above natural (percentage points)	Principal limitation
Natural depletion	5	0	26.68	0.00	Pressure decline and late free-gas mobility
Water injection	5	4	48.61	21.93	Water breakthrough and produced-water handling
Gas injection	3	2	28.16	1.48	Early gas breakthrough; GOR limit exceeded
WAG injection	5	6	50.73	24.05	Operational complexity, compression, switching, injectivity

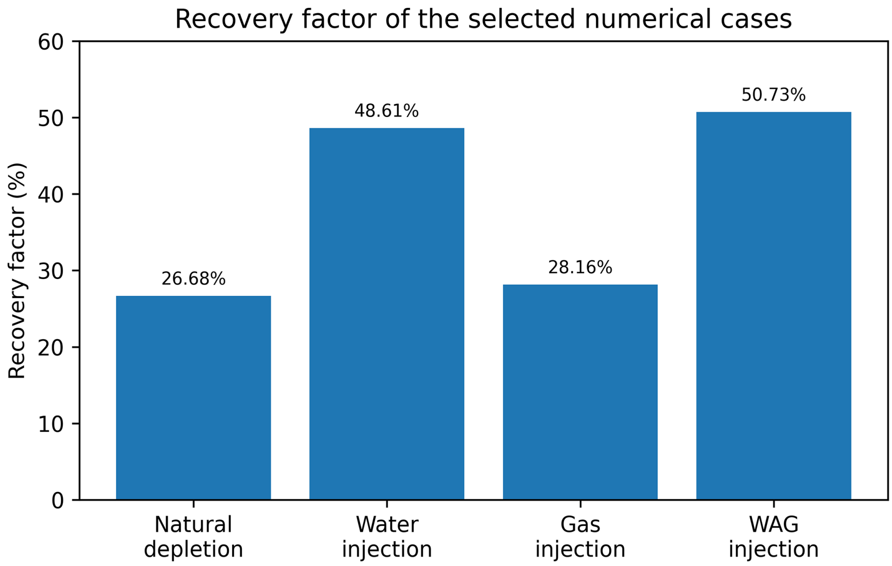

Figure 10. Recovery factors for the selected numerical cases.

The selected-case recovery factors are 26.68% for natural depletion, 48.61% for water injection, 28.16% for gas injection, and 50.73% for WAG. The selected water case uses four injectors and the WAG case uses six injectors. For WAG, the technical comparison uses the simulator-reported recovery factor; the cumulative-barrel value in one archived summary is omitted because it does not reconcile with the stated OOIP and recovery factor. The economic performance of the selected cases is summarised in **Table 10**, and their NPV values are compared in **Figure 11**.

Water injection is the preferred overall economic case because it generates the highest NPV (1,785 MM$), highest IRR (34.78%), and highest reported NPV/investment ratio (1.52), while retaining a short payback of 3.844 years. Gas injection has the shortest payback period at 3.703 years, not water injection. Its lower recovery and NPV prevent it from ranking first. WAG has the second-highest NPV and the highest recovery, but its additional injectors, compressor, and switching requirements reduce its economic advantage relative to water injection.

Table 10. Economic performance of the selected cases.

Scheme	Investment (MM$)	Reported PI = NPV/investment	NPV (MM$)	IRR (%)	PBP (years)	Overall rank
Natural depletion	1070	0.77	825	27.62	4.12065	4
Water injection	1178	1.52	1785	34.78	3.84431	1
Gas injection	1078	0.89	963	30.91	3.70299	3
WAG injection	1294	1.31	1694	32.29	4.11149	2

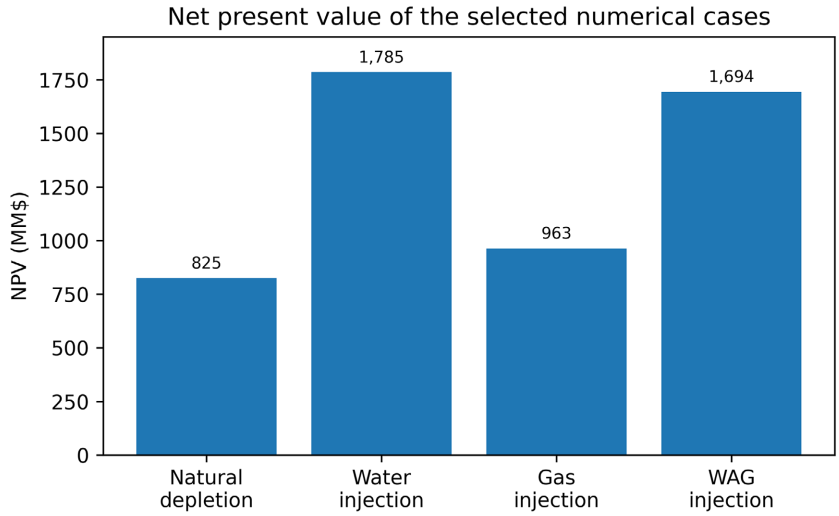

Figure 11. Net present value of the selected numerical cases.

An operational-complexity score was used only as a qualitative visualization. The score increases with well count, gas compression, produced-fluid handling, phase switching, and surveillance requirements: natural depletion = 1, water injection = 3, gas injection = 4, and WAG = 5. It is not an independent economic metric and does not replace the reported cash-flow indicators. The combined technical-economic-operational comparison is presented in **Figure 12**. Comparison with previous economic studies. The ranking illustrates the principle emphasized by EOR economic evaluations: the technically highest recovery case is not necessarily the maximum-value case once drilling, compression, facilities, and operating complexity are included [7]. Waterflood optimization studies likewise show that well count and placement can materially affect value even where recovery differences are small [12]. The result supports integrated screening rather than selection by recovery factor or payback period alone.

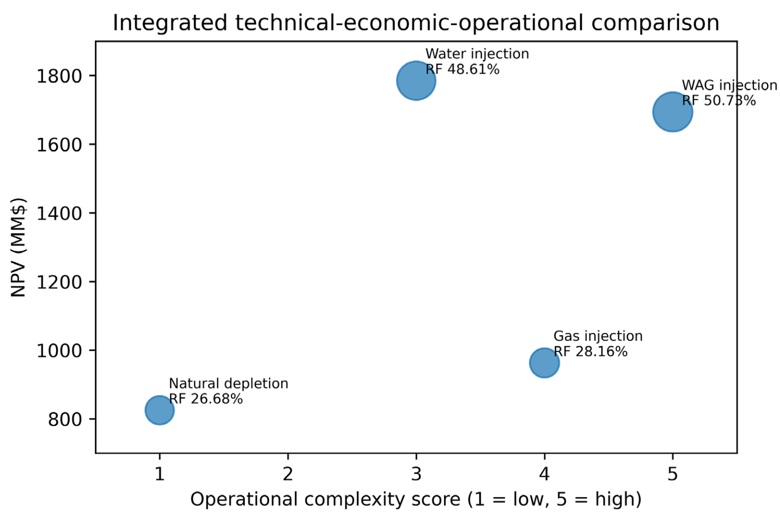

Figure 12. Integrated technical-economic-operational comparison. Bubble size is proportional to recovery factor; complexity scores are qualitative and defined in the text.

5. Study Limitations and Uncertainty

The study is a comparative development-planning exercise based on an academic Brent East sector model. It is not a complete Alwyn North full-field model, and it does not represent every structural panel, facility interaction, or field operating constraint.

The exact ACTNUM-active count, numerical fault transmissibility multipliers, detailed I/J/K coordinates for all new wells, completion-cell lists, and aquifer-only pore volume were not recoverable from the available archived model and calculation records. These quantities are explicitly labeled unavailable rather than reconstructed from figures.

No complete observed pressure, oil-rate, water-cut, or GOR time series was available. A formal history match, quantitative match errors, and acceptance criteria were therefore not possible. Forecast uncertainty associated with fault communication, water-zone strength, permeability anisotropy, relative permeability, and well productivity remains material.

The WAG case is time controlled and does not contain a single fixed pore-volume slug or WAG ratio. One archived summary also gives a cumulative-barrel value that does not reconcile with the stated OOIP and recovery factor; the comparison therefore uses the simulator-reported recovery factor and omits the conflicting cumulative volume.

Economic calculations use a constant March 2023 oil price and simplified development costs. Inflation, price volatility, abandonment, decommissioning, detailed water-disposal costs, gas value, carbon costs, and fiscal changes were not modeled. The reported NPV/investment ratio is NPV divided by total investment and is not the conventional profitability-index definition.

The selected gas case exceeded the stated GOR limit in the archived forecast. A field implementation would need revised gas-handling capacity or operating controls. Sensitivity analysis should be expanded to include fault sealing, water-zone pore volume, Tarbert interlayer transmissibility, permeability anisotropy, oil price, OPEX, and injection capacity.

6. Conclusions

This study compared natural depletion, water injection, immiscible gas injection, and WAG in the Brent East panel of the Alwyn North Field using a common ECLIPSE E100 sector model and discounted-cash-flow framework. The model description reports the 36 × 51 × 18 geometrical grids, the available interpretation of 17 effective reservoir layers, nominal cell dimensions, documented binary fault behavior, initial pressure, bubble-point pressure, and OOIP, while clearly identifying unavailable or conflicting deck-level quantities. Water support is represented by gridded water-bearing cells rather than an undocumented analytical aquifer, and the absence of formal history matching is explicitly acknowledged.

The selected-case recovery factors are 26.68% for natural depletion, 48.61% for water injection, 28.16% for gas injection, and 50.73% for WAG. Water injection provides the largest economically efficient recovery increment through pressure maintenance and improved sweep. Continuous immiscible gas injection is limited by early breakthrough and high GOR. WAG produces the highest technical recovery but adds only 2.12 percentage points above water injection and requires greater investment and operating complexity.

Water injection is the preferred development strategy under the stated assumptions because it has the highest NPV (1,785 MM$) and IRR (34.78%). Gas injection has the shortest payback period (3.703 years), while WAG ranks second economically and first technically. The findings demonstrate that development selection should integrate recovery, well configuration, operability, facility constraints, and cash flow rather than rely on a single technical or financial indicator.

Future work should use the original ECLIPSE deck and observed field data to quantify active cells, fault transmissibility, water-zone pore volume, well completions, and history-match quality. Ensemble-based uncertainty analysis and optimization should then be applied before field implementation.

Data and Model Availability

The analysis was reconstructed from archived model documentation, simulation outputs, and economic calculation records available to the authors. The original complete ECLIPSE deck, simulator restart files, and full observed production-history database were not available. The limitations arising from unavailable deck-level and historical data are disclosed in Sections 3.1, 3.3, and 5.

CRediT Authorship Contribution Statement

Franck-Hilaire Essiagne: Conceptualization, Methodology, Software, Validation, Formal analysis, Investigation, Visualization, Writing original draft. Kouassi Louis Kra: Conceptualization, Methodology, Software, Validation. Moussa Camara: Supervision, Resources, Writing—review and editing.

Conflicts of Interest

The authors declare no conflicts of interest regarding the publication of this paper.

References

[1] Druetta, P., Tesi, P., De Persis, C. and Picchioni, F. (2016) Methods in Oil Recovery Processes and Reservoir Simulation. *Advances in Chemical Engineering and Science*, **6**, 39-435. https://doi.org/10.4236/aces.2016.64039

[2] Anvari, S. (2021) An Overview of Oil Well Drilling Problems in Shale Formations (Case Study: Asmari Reservoir). *Geosciences and Engineering*, **9**, 116-127. https://doi.org/10.33030/geosciences.2021.14.116

[3] Ozowe, W., Daramola, G.O. and Ekemezie, I.O. (2024) Petroleum Engineering Innovations: Evaluating the Impact of Advanced Gas Injection Techniques on Reservoir Management. *Magna Scientia Advanced Research and Reviews*, **11**, 299-310. https://doi.org/10.30574/msarr.2024.11.1.0094

[4] Sikiru, S., *et al*. (2023) Recent Advance and Prospect of Enhanced Oil Recovery Mech-

anisms in Reservoir Sandstone. https://doi.org/10.20944/preprints202309.1654.v2

[5] Mohammadi, M.H., Kulakhmetovna, Y.A. and Joia, R. (2024) An Overview of Oil Recovery Techniques: From Primary to Enhanced Oil Recovery Methods. *Journal for Research in Applied Sciences and Biotechnology*, **3**, 291-301. https://doi.org/10.55544/jrasb.3.1.48

[6] Salles, J.L.M., de Azevedo, R.C. and de Tomi, G. (2014) Elaboration of Reservoir Simulation Software for Academic Purpose. *Materials Science Forum*, **805**, 409-414. https://doi.org/10.4028/www.scientific.net/msf.805.409

[7] Zekri, A.Y., Jerbi, K.K. and El-Honi, M. (2000) Economic Evaluation of Enhanced Oil Recovery. *International Oil and Gas Conference and Exhibition in China*, Beijing, 7-10 November 2000, SPE-64727-MS. https://doi.org/10.2118/64727-ms

[8] Alvarado, V. and Manrique, E. (2010) Enhanced Oil Recovery: An Update Review. *Energies*, **3**, 1529-1575. https://doi.org/10.3390/en3091529

[9] Amadi, A.H., Raphael, O. and Ebube, O.F. (2020) Comparative Analysis of Water Drive, Gas Drive and Natural Drive Mechanism for Oil Production Using Alwyn North Field as a Case Study. *European Journal of Engineering Research and Science*, **5**, 479-484. https://doi.org/10.24018/ejers.2020.5.4.1892

[10] Zene, M.T.A.M., Hasan, N., Jiang, R., Zhenliang, G. and Abdullah, N. (2021) Evaluation of Reservoir Performance by Waterflooding: Case Based on Lanea Oilfield, Chad. *Journal of Petroleum Exploration and Production Technology*, **11**, 1339-1352. https://doi.org/10.1007/s13202-021-01109-1

[11] Bhattacharyya, S. and Vyas, A. (2022) A Novel Methodology for Fast Reservoir Simulation of Single-Phase Gas Reservoirs Using Machine Learning. *Heliyon*, **8**, e12067. https://doi.org/10.1016/j.heliyon.2022.e12067

[12] Farahi, M.M.M., Ahmadi, M. and Dabir, B. (2021) Model-Based Water-Flooding Optimization Using Multi-Objective Approach for Efficient Reservoir Management. *Journal of Petroleum Science and Engineering*, **196**, Article ID: 107988. https://doi.org/10.1016/j.petrol.2020.107988

[13] Wu, R., Wei, B., Li, S., Zhang, Y. and Luo, Q. (2023) Enhanced Oil Recovery in Complex Reservoirs: Challenges and Methods. *Advances in Geo-Energy Research*, **10**, 208-212. https://doi.org/10.46690/ager.2023.12.07

[14] Sharma, M.M., Pang, S., Wennberg, K.E. and Morgenthaler, L.N. (2000) Injectivity Decline in Water-Injection Wells: An Offshore Gulf of Mexico Case Study. *SPE Production & Facilities*, **15**, 6-13. https://doi.org/10.2118/60901-pa

[15] Cui, X., Chen, Z., Wang, R., Han, Y., He, X. and Lei, Z. (2024) Optimal Design of Gas Injection Development Method for Enhanced Recovery in Terrestrial Shale Oil Reservoir. *Frontiers in Energy Research*, **12**, Article 1397417. https://doi.org/10.3389/fenrg.2024.1397417

[16] Afzali, S., Rezaei, N. and Zendehboudi, S. (2018) A Comprehensive Review on Enhanced Oil Recovery by Water Alternating Gas (WAG) Injection. *Fuel*, **227**, 218-246. https://doi.org/10.1016/j.fuel.2018.04.015

[17] Inglis, I. and Gerard, J. (1991) The Alwyn North Field, Blocks 3/9a, 3/4a, UK North Sea. *Geological Society*, *London*, *Memoirs*, **14**, 21-32. https://doi.org/10.1144/gsl.mem.1991.014.01.03

[18] Bazin, B., Brosse, É. and Sommer, F. (1997) Chemistry of Oil-Field Brines in Relation to Diagenesis of Reservoirs—2. Reconstruction of Palaeo-Water Composition for Modelling Illite Diagenesis in the Greater Alwyn Area (North Sea). *Marine and Petroleum Geology*, **14**, 497-511. https://doi.org/10.1016/s0264-8172(97)00005-6

[19] Tomasso, M., Underhill, J.R., Hodgkinson, R.A. and Young, M.J. (2008) Structural Styles and Depositional Architecture in the Triassic of the Ninian and Alwyn North Fields: Implications for Basin Development and Prospectivity in the Northern North Sea. *Marine and Petroleum Geology*, **25**, 588-605. https://doi.org/10.1016/j.marpetgeo.2007.11.007

[20] Harker, S.D., Richardson, G., Sides, L.E. and Cooper, R. (2003) Alwyn North Triassic Main Gas-Condensate: Drilling Deeper Promotes Production. *Petroleum Geoscience*, **9**, 133-143. https://doi.org/10.1144/1354-079302-550

[21] Hampson, G.J., Sixsmith, P.J. and Johnson, H.D. (2004) A Sedimentological Approach to Refining Reservoir Architecture in a Mature Hydrocarbon Province: The Brent Province, UK North Sea. *Marine and Petroleum Geology*, **21**, 457-484. https://doi.org/10.1016/s0264-8172(03)00094-1

[22] Hubans, C., Rapin, M., Ottlé, J.F., Manin, M., Harker, S.D., Richardson, G., *et al.* (2003) 4D Using Legacy Seismic Data on the Alwyn North Oil Field. *Petroleum Geoscience*, **9**, 15-24. https://doi.org/10.1144/1354-079302-538

[23] Livera, S.E. and Caline, B. (1990) The Sedimentology of the Brent Group in the *Cormorant* Block IV Oilfield. *Journal of Petroleum Geology*, **13**, 367-396. https://doi.org/10.1111/j.1747-5457.1990.tb00855.x

[24] Girard, J.P., Munz, I.A., Johansen, H., Hill, S. and Canham, A. (2001) Conditions and Timing of Quartz Cementation in Brent Reservoirs, Hild Field, North Sea: Constraints from Fluid Inclusions and SIMS Oxygen Isotope Microanalysis. *Chemical Geology*, **176**, 73-92. https://doi.org/10.1016/s0009-2541(00)00350-8

[25] Hogg, A.J.C., Pearson, M.J., Fallick, A.E. and Hamilton, P.J. (1995) An Integrated Thermal and Isotopic Study of the Diagenesis of the Brent Group, Alwyn South, U.K. North Sea. *Applied Geochemistry*, **10**, 531-546. https://doi.org/10.1016/0883-2927(95)00024-0

[26] Baccar, M.B., Fritz, B. and Brévart, O. (1993) Geochemical Modelling of Late Diagenetic Processes in the Brent Sandstone, Alwyn South Area (East Shetland Basin, North Sea). *Chemical Geology*, **109**, 135-147. https://doi.org/10.1016/0009-2541(93)90067-s

[27] Tseng, H.Y. and Pottorf, R.J. (2002) Fluid Inclusion Constraints on Petroleum PVT and Compositional History of the Greater Alwyn—South Brent Petroleum System, Northern North Sea. *Marine and Petroleum Geology*, **19**, 797-809. https://doi.org/10.1016/s0264-8172(02)00088-0

[28] Hogg, A.J.C., Hamilton, P.J. and Macintyre, R.M. (1993) Mapping Diagenetic Fluid Flow within a Reservoir: K Ar Dating in the Alwyn Area (UK North Sea). *Marine and Petroleum Geology*, **10**, 279-294. https://doi.org/10.1016/0264-8172(93)90110-e

[29] Blanchet, A., Pagel, M., Walgenwitz, F. and Lopez, A. (2003) Microspectrofluorimetric and Microthermometric Evidence for Variability in Hydrocarbon Fluid Inclusions in Quartz Overgrowths: Implications for Inclusion Trapping in the Alwyn North Field, North Sea. *Organic Geochemistry*, **34**, 1477-1490. https://doi.org/10.1016/j.orggeochem.2003.08.003

[30] Cheraghi, Y., Kord, S. and Mashayekhizadeh, V. (2021) Application of Machine Learning Techniques for Selecting the Most Suitable Enhanced Oil Recovery Method; Challenges and Opportunities. *Journal of Petroleum Science and Engineering*, **205**, Article ID: 108761. https://doi.org/10.1016/j.petrol.2021.108761

[31] Vaziri, P., Ahmadi, S., Daneshfar, F., Sedaee, B., Alimohammadi, H. and Rasaei, M.R. (2024) Machine Learning Techniques in Enhanced Oil Recovery Screening Using Semisupervised Label Propagation. *SPE Journal*, **29**, 4557-4578.

https://doi.org/10.2118/221475-pa

[32] Kou, Z., Wang, H., Alvarado, V., Fred McLaughlin, J. and Austin Quillinan, S. (2022) Method for Upscaling of CO_2 Migration in 3D Heterogeneous Geological Models. *Journal of Hydrology*, **613**, Article ID: 128361. https://doi.org/10.1016/j.jhydrol.2022.128361

[33] Essiagne, F.H., Kra, K.L., Camara, M. and Kouadio, K.E. (2025) Assessing the Impact of Reservoir Heterogeneity on Carbon Capture and Storage Feasibility through Numerical Simulation. *Open Journal of Geology*, **15**, 867-896. https://doi.org/10.4236/ojg.2025.1512045

[34] Fuentes-Cruz, G. and Vásquez-Cruz, M.A. (2022) Reservoir Performance Analysis through the Material Balance Equation: An Integrated Review Based on Field Examples. *Journal of Petroleum Science and Engineering*, **208**, Article ID: 109377. https://doi.org/10.1016/j.petrol.2021.109377

[35] Tetteh, M., Li, L. and Davis, A. (2024) Leveraging Deep Learning with Progressive Growing GAN and Ensemble Smoother with Multiple Data Assimilation for Inverse Modeling. *Advances in Water Resources*, **187**, Article ID: 104680. https://doi.org/10.1016/j.advwatres.2024.104680

[36] Hurst, W. (1943) Water Influx into a Reservoir and Its Application to the Equation of Volumetric Balance. *Transactions of the AIME*, **151**, 57-72. https://doi.org/10.2118/943057-g

[37] Al-Mahasneh, M., Al-Khasawneh, H.E., Al-Zboon, K., Al-Mahasneh, M. and Aljarrah, A. (2023) Water Influx Impact on Oil Production in Hamzeh Oil Reservoir in Northeastern Jordan: Case Study. *Energies*, **16**, Article 2126. https://doi.org/10.3390/en16052126